Electronic structure of rare earth bismuthides

2003 J. Phys.: Condens. Matter 15 3701

(http://iopscience.iop.org/0953-8984/15/22/305)

INSTITUTE OF PHYSICS PUBLISHING JOURNAL OF PHYSICS: CONDENSED MATTER

J. Phys.: Condens. Matter **15** (2003) 3701–3716 PII: S0953-8984(03)56021-0

Electronic structure of rare earth bismuthides

M Drzyzga[1], J Szade[1,3], J Deniszczyk[1,2] and T Michalecki[1,2]

[1] A Chełkowski Institute of Physics, University of Silesia, Uniwersytecka 4, 40-007 Katowice, Poland
[2] Institute of Physics and Chemistry of Metals, University of Silesia, Bankowa 12, 40-007 Katowice, Poland

E-mail: szade@us.edu.pl

Received 13 November 2002, in final form 21 March 2003
Published 23 May 2003
Online at stacks.iop.org/JPhysCM/15/3701

Abstract

The electronic structure of rare earth bismuthides—Gd_4Bi_3, Tb_4Bi_3 and R_5Bi_3 (R = Gd, Tb, Dy, Ho, Er)—has been investigated with use of x-ray and ultraviolet photoelectron spectroscopies and calculated with the tight-binding linear muffin-tin orbital method. The spectra simulated on the basis of *ab initio* results reproduce correctly the experimental ones. This enabled analysis of the character of the electronic states, their hybridization and influence on magnetic properties. The temperature dependence of the valence band photoemission of ferromagnetic Gd_4Bi_3 and Tb_4Bi_3 has been studied and compared to the results obtained with the spin-polarized, non-polarized and open core methods of calculation.

1. Introduction

There are only a few studies of the electronic structure of rare earth compounds with bismuth reported so far. Gd monopnictides, including GdBi, were investigated with many techniques including x-ray photoemission [1–3]. The relations between the magnetic properties and electronic structure have been found for polycrystalline Gd_4Bi_3 and Gd_5Bi_3 [4]. Recently, we have reported on the crystallographic and magnetic properties of Tb_4Bi_3 and R_5Bi_3 (for R = Tb, Dy, Ho and Er) [5]. The investigated R_5Bi_3 compounds exhibit very unusual magnetic properties, especially thermomagnetic effects at low temperatures. Tb_4Bi_3, which has a different crystal structure, orders ferromagnetically at about 200 K. Knowledge about the electronic structure of such compounds may help in explaining their peculiar properties. The analysis of the photoemission from valence band and core levels has been used to draw conclusions about bonding and charge transfer in a large group of Gd intermetallic compounds [6, 7].

[3] Author to whom any correspondence should be addressed.

In this paper we report on the experimental and theoretical investigation of electronic structure of Gd_4Bi_3, Tb_4Bi_3 and R_5Bi_3 (R = Gd, Tb, Dy, Ho, Er). The valence band in the x-ray photoelectron spectroscopy (XPS) and ultraviolet photoelectron spectroscopy (UPS) regime and core level photoemission have been studied. The analysis of the core level photoemission will be published elsewhere.

Electronic structure of the bismuthides was calculated with the use of the tight-binding linear muffin-tin orbital method in the atomic sphere approximation (TB-LMTO-ASA). The spin-polarized, non-polarized and frozen core methods of calculations have been used and discussed in relation to magnetic properties and temperature dependent photoemission data from Gd_4Bi_3 and Tb_4Bi_3.

2. Experimental details

The samples have been obtained within the procedure which has been described in our earlier papers on rare earth bismuthides [4, 5]. Two-step induction melting has been used. Samples of R_5Bi_3 (R = Tb, Dy, Ho, Er) were annealed for one week at 1000 °C, in vacuum. The structure and composition of the samples have been checked with use of x-ray diffraction, scanning electron microscopy and Auger electron spectroscopy [5].

All the R_5Bi_3 (R = Gd, Tb, Dy, Ho and Er) samples exhibit the orthorhombic Y_5Bi_3 type of structure (space group *Pnma*). For Tb_5Bi_3 the lattice constants are $a = 8.170$ Å, $b = 9.487$ Å and $c = 11.968$ Å. For other compounds they are slightly reduced according to the lanthanide contraction [5]. Gd_4Bi_3 and Tb_4Bi_3 crystallize in the cubic anti-P_4Th_3 type of structure (space group $I\bar{4}3d$). The lattice constant is 9.3215 Å for Gd_4Bi_3 and 9.320 Å for Tb_4Bi_3. The structure is relatively loosely packed; the packing factor is about 60%. The unit cell of the '4–3' compounds consists of 2 fu (14 atoms) whereas in the unit cell of the '5–3' structure there are four formula units (32 atoms).

The XPS measurements were performed with a Physical Electronics PHI 5700 ESCA spectrometer, using monochromatized Al Kα radiation. The vacuum level during the measurements was about 10^{-10} Torr. The samples were cleaved or scraped with a diamond file in the UHV chamber just before taking the spectra. For some samples sputtering with a low energy Ar ion beam (up to 1.5 kV) was necessary to ensure that the surface was free of contaminants. The influence of sputtering on chemical composition and on the shape of the peaks was checked. The level of oxygen and carbon contamination was controlled during the measurements by monitoring C 1s and O 1s photoemission levels or O and C Auger transitions.

The band-structure calculations were carried out with the use of the tight-binding linear muffin-tin orbital (TB-LMTO) method of Andersen *et al* [8]. The calculations were scalar relativistic, without the spin–orbit interaction. The exchange–correlation (XC) potential was taken within the local spin-density approximation (LSDA), with the use of the von Barth–Hedin [9] parametrization, the explicit form of which was cited in e.g. [10]. To account for the non-uniformity of the 4f and 3d electronic charge distribution, important in the investigated systems, the generalized gradient correction to the LSDA XC potential was applied in the form derived by Langreth, Mehl and Hu (LMH) [11]. In the TB-LMTO method the crystal potential is modelled within the atomic-sphere approximation (ASA).

Within this approximation the atomic potentials, inside the Wigner–Seitz (WS) spheres, are considered spherically symmetric. Outside the WS spheres (in the interstitial region) the potential is taken as constant (V_{MTZ}). The kinetic energy ($E_i^k = E_i - V_{MTZ}$) is assumed negligibly small in that region. To diminish the errors generated by the last approximation ($E_i^k \approx 0$) the WS spheres are assumed to fill the unit cell volume so that their volumes obey the volume equation $\frac{4\pi}{3}\sum_i (r_{WS}^i)^3 = V_{UC}$, where r_{WS}^i stands for the radius of the ith

atomic WS sphere and V_{UC} is the unit cell volume. In every case the volume equation forces the WS spheres to overlap, which results in an additional errors on the course of the band structure calculations. For structures with densely packed unit cells (as in the fcc, bcc and hcp structures), where the total volume of the overlap regions is of the order of a few per cent of the unit cell volume, the overlap O_{WS} $(=(r^i_{WS} + r^j_{WS} - d_{ij})/d_{ij})$ of the WS spheres separated by d_{ij} is usually less than 15%. For small overlaps ($O_{WS} < 20\%$) the errors resulting from the ASA can be significantly reduced by the inclusion of the *combined correction* terms [8] to the one-electron Hamiltonian and overlap matrices (which procedure is implemented in the TB-LMTO method). For *open* structures, with small packing, it is usually impossible to fill the unit cell space with WS spheres with the overlap O_{WS} less than 20%. In such cases it is common practice to consider empty spheres (ESs) (artificial, spherically symmetric atoms with $Z = 0$) filling up the unit cell interstitial voids. The introduction of the ESs in place of the interstitial regions with non-spherically symmetric potential is well justified for structures with high symmetry.

Among the investigated structures with '4–3' and '5–3' compositions only the cubic '4–3' structure is too loosely packed for the radii of the atomic WS spheres to obey simultaneously both the volume and overlap requirements underlying the ASA approximation. To overcome the WS sphere overlap problem occurring in RE_4Bi_3 compounds the calculations were performed on the body-centred, cubic unit cells with the basis consisting of atomic WS spheres (14 atoms) and six ESs. The volume of the ESs is about 16% of the unit cell volume. The RE_5Bi_3 structure is much more densely packed than the '4–3' one. The WS sphere overlap O_{WS} satisfies the ASA requirements and the total volume overlap was obtained to be less than 10%. Consequently, in the band calculations for the '5–3' structures no ESs were needed. For all compounds the band structure calculations have taken into account the *combined correction* terms.

The aim of our band structure calculations was to get insight into the details of the electronic structure of R_4Bi_3 and R_5Bi_3 compounds in the magnetic state and attempt to explain the changes in the electronic structure upon magnetic transitions observed experimentally for R_4Bi_3 (R = Gd and Tb). From the standpoint of the *ab initio* methods of the electronic structure calculations the description of magnetic transitions in rare-earth-based materials is impossible. The magnetic transition in localized magnetic materials is the thermodynamic effect of collective character. The paramagnetic state of the RE-based systems can be viewed as the collection of the randomly oriented localized 4f moments of RE ions embedded in the sea of conduction electrons with no long-range magnetic order. Because of single-electron and ground-state character, the applied TB-LMTO method of electronic structure calculations cannot account for all these effects.

In the electronic structure calculations for rare-earth-based materials carried out in the non-spin-polarized mode (simulating the paramagnetic state) the 4f-shell states treated as band states form a narrow band located at the Fermi level. Hybridization of these (erroneously located) 4f states with other bands (mainly of d character) significantly perturbs their shape, leading to the occurrence of gaps and peaks in the vicinity of the Fermi level.

There are two possible ways of solving this unphysical picture: to definitely remove the 4f electrons from the system or to shift them far below the Fermi energy. Following the first method one can simulate the changes of band structure upon the magnetic transition by determining the non-magnetic electronic structure of the isostructural compounds with R ions replaced by yttrium. The other approach is often called the *frozen core* method and consists in forcing the 4f states to be of core character. In this way the 4f-band hybridization is excluded and the number of 4f electrons is then fixed so there is no charge exchange with valence states.

In the standard band structure calculations (no frozen-core approximation) the initial electronic configurations of constituent atoms were taken from the periodic table. In the course

of calculations the valence state basis set of each atom was assumed to consist of all s, p, d and f states (16 wavefunctions per atom and spin). The states taken additionally into account in the valence state basis set, but absent in the free atom electronic configurations (e.g. for the Gd 6p and Bi 5f6d states), were treated by means of the down-folding procedure [8]. The structural data, like space group, atomic positions and lattice parameters, were taken from the experiment [4, 5]. The self-consistent calculations were performed for more than 27 k-points in the irreducible part of the Brillouin zone (IBZ), which, because of the large dimensions of the unit cell of both structures, was sufficient to gain total energy convergence. To get a better statistics, for the purposes of the density of states (DOS) plotting and the simulations of the XPS and UPS spectra, additional iterations with more than 64 k-points in the IBZ were done. Based on the calculated single-electron band energies (ε_{jk}) the partial (atomic-, spin- and orbital-resolved) DOS was calculated by means of the standard tetrahedron method [12].

In a one-step model of photoemission (neglecting scattering of photoelectrons) the bulk state contribution to the XPS and UPS valence band spectra, in a crude approximation, can be related to the partial DOS of the structure. The XPS (UPS) spectra presented in this paper were simulated by convolution of the calculated partial DOS contributions by Lorentzians (with a half-width of 0.35 eV for XPS and 0.2 eV for UPS) and then multiplication by the corresponding cross-sections taken from [13]. Such simulations do not take into account the final state effects and influence of the surface. Despite the crude approximations, the overall agreement of spectra simulated in this way and measured spectra is usually quite good [14]. The method allows for the identification of the most important contributions to the observed valence band photoemission spectra.

3. Results and discussion

3.1. Photoemission

The XPS spectra of the valence band of Tb_4Bi_3 and Tb_5Bi_3 are shown in figure 1, where the spectra for the pure elements are added. Both compounds exhibit similar shape of the valence band and the slight difference is visible mainly in the vicinity of the Fermi level. The inset to the figure 1 shows that Tb_4Bi_3 has a higher intensity than Tb_5Bi_3 in the binding energy (BE) range 0–1 eV. This effect is very similar to the difference found between ferromagnetic Gd_4Bi_3 and Gd_5Bi_3, which orders magnetically at much lower temperature [4]. Both Tb compounds exhibit a pronounced maximum at about 3.5 eV. In the case of Tb compounds this peak may originate mainly from the final photoemission state of the Tb 4f shell ($^8S_7$), which is however shifted to higher BE by more than 1 eV from its position in Tb metal. The rest of the 4f multiplet is also shifted by more than 1 eV. Another characteristic feature of the 4f multiplet is a clear increase of the line-width of the component lines. This also concerns other Tb core levels whereas the Bi lines show similar line-width to the one found for the single-crystalline pure Bi. This means that the photo-hole relaxation process depends on the chemical state of the Tb atom and changes with the modifications of the valence band. The effect will be described elsewhere based on the photoemission results from the core levels. The large chemical shifts for Tb lines and strong modification of the valence band with respect to the pure elements shows that bonding with Bi is strong and does not have only metallic character. One may expect a significant charge transfer from Tb atoms. The calculations described further in the text confirm this hypothesis at least for Tb_4Bi_3 (table 1). The position of the Bi lines is hardly changed in relation to Bi metal. There is a small negative shift which may be related to the increase of the calculated total charge at the Bi atoms (table 1). The effect is very similar to the one found in Gd_4Bi_3.

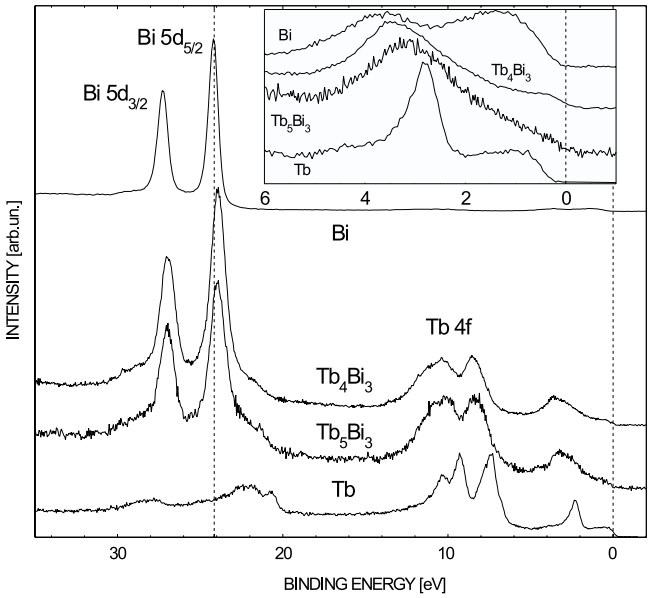

Figure 1. Valence band XPS spectra for Tb_4Bi_3 and Tb_5Bi_3. The inset shows the region close to the Fermi level. Spectra of Tb and its bismuthides are normalized with respect to the intensity of the Tb 4f level.

Table 1. Results of the TB LMTO spin-polarized (FM), non-magnetic (NM) and frozen core (OC) calculations for Gd_4Bi_3 and Tb_4Bi_3. Partial atomic occupations are denoted as n, magnetic moments μ [μ_B/atom] and DOS at Fermi energy $D(\varepsilon_F)$ ((eV atom)$^{-1}$), with separated orbital contributions (s + p, d). ΔQ means the charge transfer for particular atoms.

	Gd_4Bi_3						Tb_4Bi_3					
	FM		NM		OC		FM		NM		OC	
	Gd	Bi	Gd	Bi	Gd	Bi	Tb	Bi	Tb	Bi	Tb	Bi
n_{s+p}	0.737	5.3	0.69	5.3	0.6	4.6	0.6	5.54	0.529	5.58	0.7	4.6
n_d	1.28	0.217	0.9	0.17	1.7	0.3	1.03	0.253	0.73	0.2	1.6	0.3
n_f	7.21	0.065	7.7	0.06			8.31	0.079	8.68	0.08		
μ_{s+p}	0.046	0.06					0.032	0.02				
μ_d	0.296	0.057					0.11	0.015				
μ_f	6.79	0.023					5.65	0.009				
μ_{tot} (μ_B/f$_u$)	7.136	0.14					5.76	0.044				
D_{s+p}	0.4	0.69	0.083	0.33	4.67	1	0.41	0.31	0.09	0.3	0.22	0.33
D_d	4.04	0.55	0.61	0.17	0.42	0.7	2.21	0.91	0.77	0.5	2.49	0.57
$D_{tot(s+p+d)}$	4.44	1.24	0.693	0.5	5.09	1.7	2.62	1.22	0.86	0.8	2.71	0.9
ΔQ	−0.77	0.58	−0.7	0.4			−1.055	0.88	−1.06	0.87		

The charge transfer, which is obtained from calculations, is very sensitive to small changes of the atomic position in the unit cell and related to atomic sphere radii. The influence of these factors is clearly visible in the calculation for the densely packed R_5Bi_3 structure. Except Dy_5Bi_3, all R_5Bi_3 show the net charge transfer to R atoms (table 2). According to the crystallographic data Dy_5Bi_3 exhibits slightly different positions of atoms compared to other R_5Bi_3 [5]. This may be a reason fro the different behaviour of the calculated charge transfer.

Table 2. (a) Results of the spin-polarized TB LMTO calculations for Gd_5Bi_3 and Tb_5Bi_3. Partial atomic occupations are denoted as n, magnetic moments as μ (μ_B/atom) and DOS at Fermi energy as $D(\varepsilon_F)$ ((eV atom)$^{-1}$), with separated orbital contributions (s + p, d). ΔQ means the charge transfer for particular atoms. (b) Results of the spin-polarized TB LMTO calculations for Dy_5Bi_3 and Ho_5Bi_3. Partial atomic occupations are denoted as n and magnetic moments as μ (μ_B/atom), with separated orbital contributions (s + p, d). ΔQ means the charge transfer for particular atoms.

(a)	Gd_5Bi_3						Tb_5Bi_3					
	Gd1	Gd2	Gd3	Gd4	Bi1	Bi2	Tb1	Tb2	Tb3	Tb4	Bi1	Bi2
n_{s+p}	1.25	1.27	1.23	1.37	3.645	4.43	1.32	1.34	1.56	1.33	3.61	4.1
n_d	1.76	1.87	1.6	1.9	0.084	0.14	1.75	1.79	1.57	1.75	0.08	0.1
n_f	7.3	7.3	7.25	7.29	0.153	0.046	8.43	8.49	8.55	8.41	0.022	0.03
μ_{s+p}	0.07	0.05	0.03	0.09	0.055	0.05	0.06	0.05	0.08	0.07	0.01	0.01
μ_d	0.229	0.33	0.4	0.32	0.016	0.02	0.15	0.13	0.15	0.17	0.012	0.003
μ_f	6.8	6.8	6.83	6.83	0.138	0.019	5.686	5.63	5.65	5.69	0.004	0.002
μ_{tot} (μ_B)	7.13	7.19	7.3	7.23	0.209	0.089	5.89	5.81	5.87	5.92	0.026	0.015
ΔQ	0.316	0.465	0.09	0.55	−1.24	−0.39	0.52	0.62	0.68	0.5	−1.28	−0.7
D_{s+p}			0.65			0.9						
D_d			2.93			0.37						
$D_{tot(s+p+d)}$			3.58			1.27						

(b)	Dy_5Bi_3						Ho_5Bi_3					
	Dy1	Dy2	Dy3	Dy4	Bi1	Bi2	Ho1	Ho2	Ho3	Ho4	Bi1	Bi2
n_{s+p}	0.82	0.93	1.05	0.65	5.07	5.29	1.33	1.44	1.52	1.4	3.59	4
n_d	1.42	1.36	1.4	1.42	0.26	0.22	1.5	1.56	1.33	1.5	0.078	0.084
n_f	9.3	9.4	9.4	9.3	0.07	0.068	10.67	10	10.77	10.7	0.22	0.024
μ_{s+p}	0.02	0.01	0.05	0.03	0.01	0.01	0.03	0.02	0.04	0.02	0.03	0.04
μ_d	0.1	0.06	0.1	0.12	0.02	0.002	0.04	0	0.01	0.04	0.002	0.004
μ_f	4.7	4.6	4.7	4.7	0.01	0.085	3.39	3.36	3.35	3.38	0	0.002
μ_{tot} (μ_B)	4.83	4.74	4.8	4.86	0.04	0.097	3.45	3.37	3.39	3.44	0.032	0.046
ΔQ	−0.42	−0.31	−0.044	−0.38	0.41	0.57	0.49	0.77	0.63	0.6	−1.31	−0.89

For Dy_5Bi_3 the calculated charge transfer Dy → Bi (table 2(a)) could explain the chemical shift of Dy and Bi photoemission lines.

For both Tb bismuthides we performed measurements of the electronic structure at temperatures below or very close to the temperatures of magnetic transitions. The results, which include the UPS data, are shown in figures 2(a) and 3. Additionally, we performed the measurements of Gd_4Bi_3 at high temperature (426 K), so above the ferromagnetic transition (figure 2(b)). All the UPS data exhibit features which are different from the XPS ones. Generally, the states just below the Fermi level are much more pronounced in the UPS spectra. This is related to the relative changes of the photo-ionization cross sections with photon energy. In the case of Tb_4Bi_3 both XPS and UPS spectra (figure 3) show a slight increase of the intensity at about 0.7–0.9 eV when the temperature is lowered below T_C. Also at about 2.7 eV the XPS spectrum shows a bump which is not visible at room temperature. The UPS spectra do not show significant changes in this region. The spectra of Gd_4Bi_3 exhibit a different temperature dependent behaviour (figure 2(b)). The intensity at about 1 eV increases relatively at temperatures above the ferromagnetic transition. The temperature dependence of the Tb_5Bi_3 spectra is much less remarkable, probably due to the temperature of the photoemission measurement which was above to the magnetic ordering one, so the system was still in the paramagnetic state. The magnetic data show for this compound two transitions at about 100 and 60 K [5].

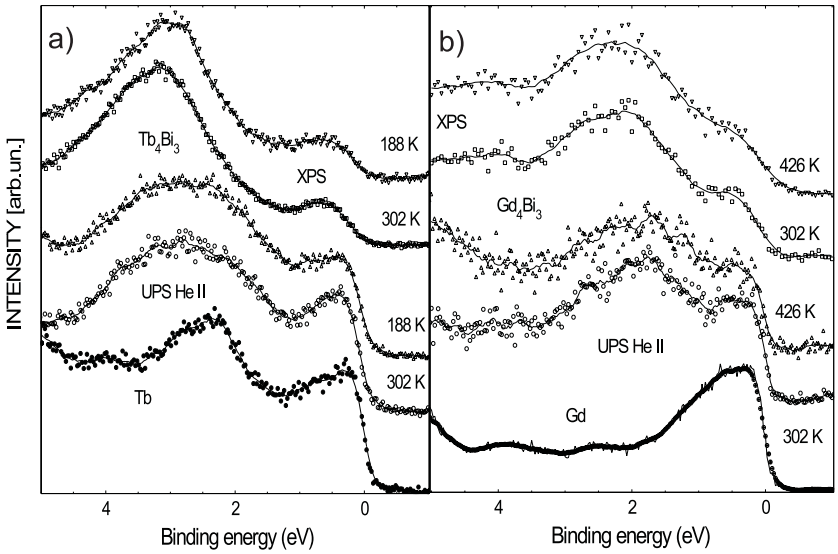

Figure 2. (a) Valence band XPS and UPS spectra for Tb_4Bi_3 obtained at various temperatures. Spectra of Tb and its bismuthides are normalized with respect to the intensity of the Tb 4f level. (b) Valence band XPS and UPS spectra for Tb_5Bi_3 obtained at various temperatures. Spectra of Tb and its bismuthides are normalized with respect to the intensity of the Tb 4f level.

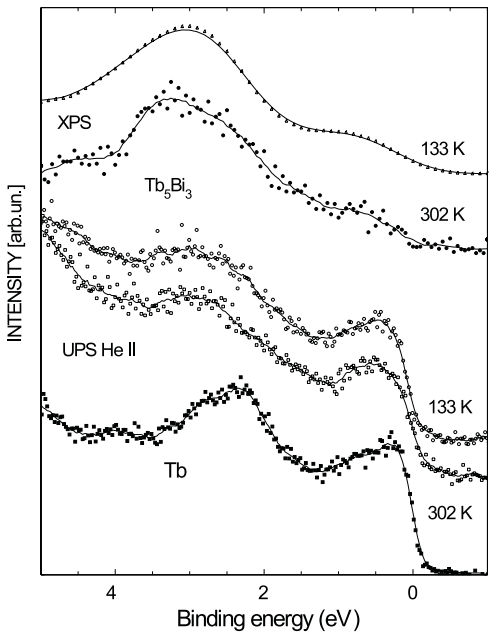

Figure 3. Valence band XPS and UPS spectra for Gd_4Bi_3 obtained at various temperatures. Spectra of Gd and its bismuthides are normalized with respect to the intensity of the Gd 4f level.

For the rest of the R_5Bi_3 (R = Dy, Ho and Er) group of compounds the photoemission studies have been limited to XPS at room temperature. The results are presented in figures 4–6. All the compounds exhibit properties similar to Tb_5Bi_3.

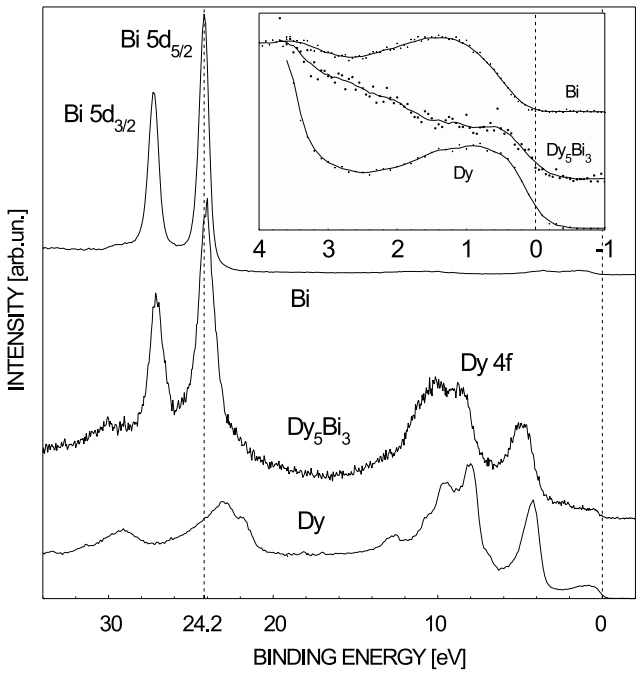

Figure 4. Valence band XPS spectra for Dy_5Bi_3. The inset shows the region close to the Fermi level. Spectra of Dy and its bismuthides are normalized with respect to the intensity of the Dy 4f level.

Similarly to the Tb compound the line-width of the peaks from the 4f multiplets increased considerably with respect to pure elements. Also the chemical shift of about 1 eV is visible. It increases from Dy to Er, indicating to some relation to the rare earth contraction and the related decrease of the unit cell [5].

The effect of 4f multiplet line broadening may be connected with the matrix elements determining the relaxation process of photoexcitation. Such matrix elements involve the valence states which are different in the compounds than in the rare earth metal. Detailed analysis of the transition probabilities is however impossible based on the experimental results and calculations performed by the LMTO method.

Discussion of the valence band photoemission spectra should take into account the possible surface effects. Due to the photoelectron mean free path one may expect a significant contribution of the surface states to the spectra in the UPS regime. It is possible that such states, which have usually lower BE than the bulk ones, cause some broadening of the spectral features, particularly from the rare earth multiplets. However the shape of the UPS spectra from the rare earth bismuthides does not allow a reasonable analysis of the possible surface components.

3.2. Calculations

Figure 7(a) illustrates the DOS for Tb_4Bi_3 obtained with the use of spin-polarized, non-magnetic and frozen core methods. The f states from Tb are not shown. Figure 8(a) shows the partial, spin- and orbital-resolved, contributions of different atoms. The distribution of the calculated states between Tb and Bi atoms is similar for all methods. For all methods an

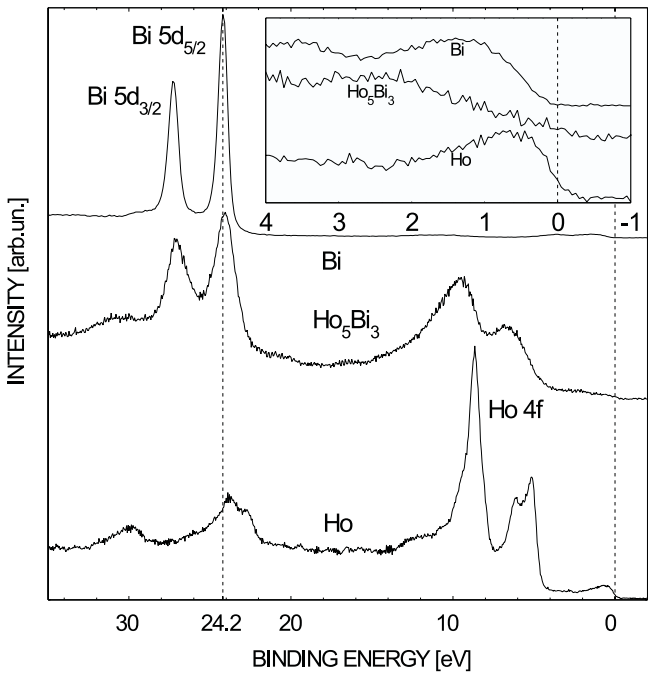

Figure 5. Valence band XPS spectra for Ho_5Bi_3. The inset shows the region close to the Fermi level. Spectra of Ho and its bismuthides are normalized with respect to the intensity of the Ho 4f level.

energy gap has been obtained of about 0.5 eV width and centred at BE of about 1 eV. The presence of the gap in the DOS obtained with various methods indicates that the origin of the gap is not related to exchange interactions. However, the width of the gap depends on the spin direction. The bottom of the conduction band is located below the Fermi energy at 0.3 eV for the minority spin and at 0.5 eV for the majority spin.

The wide band below the gap, in the energy range 2–6 eV below E_F, is formed mainly from the p states originating from Bi with some addition of the d states from Tb. Above the gap the Tb d states are dominating (figure 8(a)). These states give the largest contribution to the DOS at the Fermi level (table 1). The deep band at about -11 eV is formed mainly from Bi s states which are slightly hybridized with Tb spd states. Hybridization with Tb 4f states (not shown here for clarity) is an origin of some features visible in the DOS obtained for spin-polarized and non-spin-polarized modes of calculation in the vicinity of E_F. The 4f majority spin states are situated at about 4 eV and cause a small increase of the DOS in this area due to the hybridization. In the non-magnetic calculations the open 4f band must appear at the Fermi level and its hybridization with the conduction spd states leads to the characteristic shape of the DOS—two sharp peaks separated with a dip and a gap at the energy 0.3 eV above the Fermi level (figures 7(a), 8(a)). It should be stressed that this method of calculations cannot be applied for rare earths characterized by large 4f electron correlation energy. The results of the frozen core calculations presented in the bottom panels of figures 7(a) and 8(a) show the shape of the DOS similar to the magnetic case. However, the bottom of the main band is shifted to higher BE, which seems to be unphysical. The shape of the DOS in the vicinity of the Fermi level resembles the majority spin result in the ferromagnetic case.

The results of calculations may be compared to the experimental data obtained for temperatures below and above the Curie point (190 K) (figure 2). For the paramagnetic

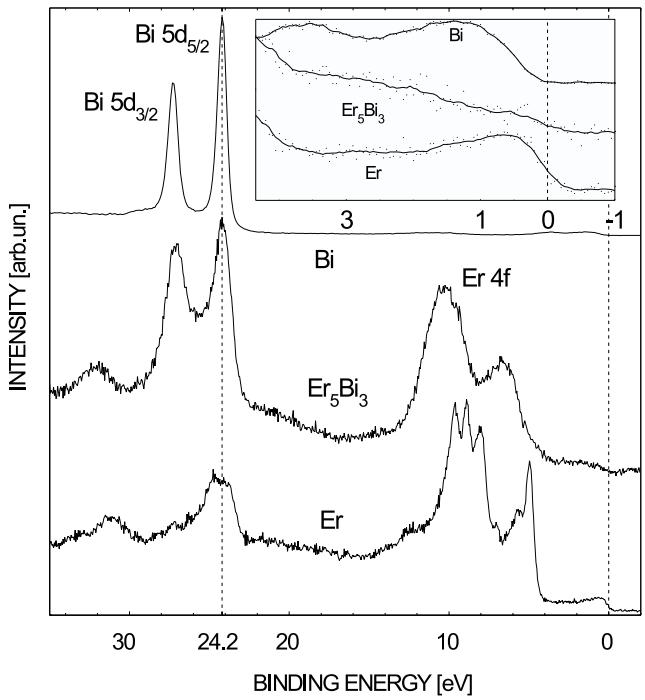

Figure 6. Valence band XPS spectra for Er_5Bi_3. The inset shows the region close to the Fermi level. Spectra of Er and its bismuthides are normalized with respect to the intensity of the Er 4f level.

case (temperature 302 K) the dip at about 1 eV is more pronounced than for the ferromagnetic case (188 K) while the bump at 0.5 eV remains almost unchanged. According to calculations this effect may be related to the exchange splitting. The frozen core calculations have shown that the energy gap in the spd DOS, located at the same energy range as for the spin-polarized DOS, is wider. This may cause deepening of the dip at 1 eV BE.

Figures 7(b) and 8(b) give the DOS for Gd_4Bi_3 calculated within three methods applied. Generally, the DOS structure is similar to that of Tb_4Bi_3. There are however some differences which can be compared to the photoemission spectra of both compounds. A clear difference can be seen in the spin-polarized DOS. Because of the larger spin momentum of the Gd 4f shell, as compared to Tb (table 1), the exchange splitting of the d conduction band is larger in Gd_4Bi_3. It leads to the narrowing of the gap in the total spin DOS of Gd_4Bi_3 which corresponds to the differences in the photoemission spectra (figures 2(a) and (b)). The conduction d-band contribution to the DOS at the Fermi level is about twice as large for Gd_4Bi_3 as for Tb_4Bi_3 (table 1). The direct comparison to the experiment is easier for Gd_4Bi_3 due the position of the 4f photoemission peak, which is situated at about 8 eV and does not overlap with other states. The calculated positions of the 4f-↑ band of the Gd atom differ significantly from the measured ones, which is a common feature of the electronic structure calculations based on the standard LSDA type of XC potential even with the gradient corrections. Too small 4f BE, and in effect relatively high non-physical contribution to the total DOS at the Fermi level coming from 4f-↓ states of Gd atoms, is the consequence of the highly non-homogeneous 4f electron charge density and modelling nature of the LSDA. A discussion of the problem is given in our previous paper [15]. In the BE range 0–4 eV, when neglecting the contribution

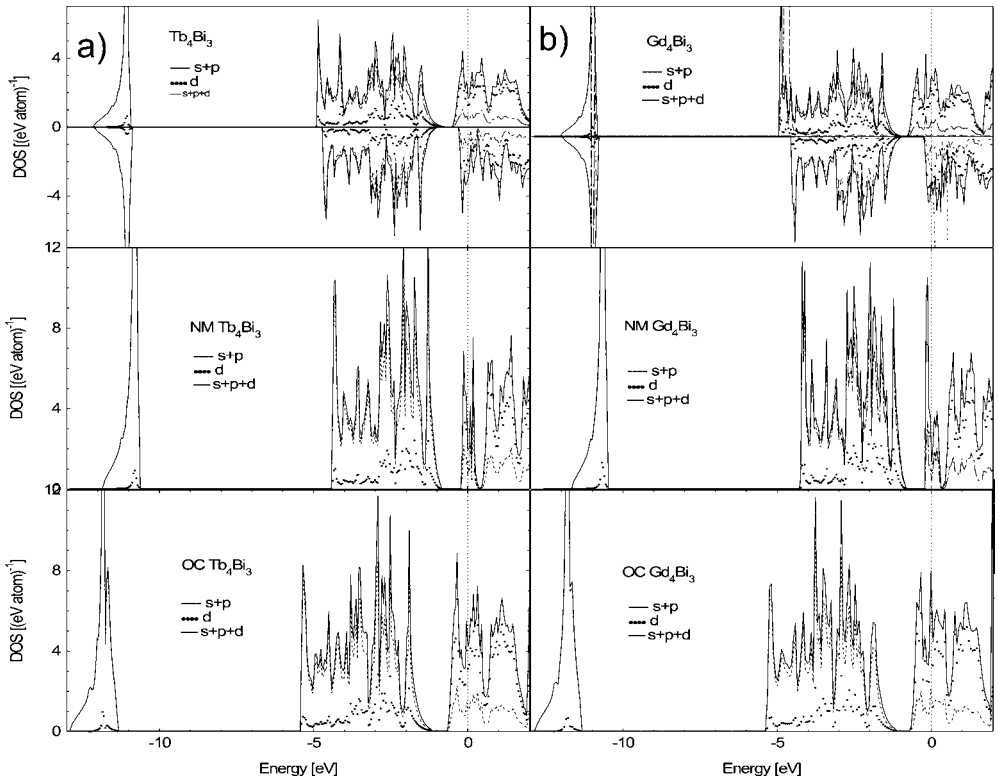

Figure 7. (a) DOS for Tb_4Bi_3 obtained with use of spin-polarized, non-magnetic and frozen (open) core (OC) methods. The f states from Tb are not shown. Vertical, dotted lines show the position of ε_F. (b) DOS for Gd_4Bi_3 obtained with use of spin-polarized, non-magnetic and frozen (open) core (OC) methods. The f states from Gd are not shown. Vertical, dotted lines show the position of ε_F.

of the Gd 4f states, the simulated XPS and UPS spectra for Gd_4Bi_3 (figure 9) fit very well to the experimental ones. In Tb_4Bi_3 one of the possible photoemission final states of the 4f band locates at BE of 3.5 eV and dominates the XPS and UPS spectra in that energy range. For that reason it is difficult to compare the shape of the valence band simulated spectra with experiment.

The temperature dependence of the experimental XPS and UPS data for Gd_4Bi_3 (figure 2(b)) differs slightly from that obtained for Tb_4Bi_3 (figure 2(a)). There is only a weak enhancement of the structure at 0.5 eV, visible mainly in XPS, when the temperature is below T_C (335 K). The difference may be related to the larger exchange splitting for Gd_4Bi_3 visible in figure 10. This splitting makes Gd_4Bi_3 close to the half-metal situation in the ferromagnetic state. The transition to the paramagnetic state causes the energy gap to shift to lower BE and the bump, visible at about 0.5 eV BE, becomes less pronounced.

It is worth mentioning that the temperature dependence of electrical resistivity of both Gd_4Bi_3 and Tb_4Bi_3 compounds is far from the classic metallic one, showing negative curvature in a large temperature range [4, 5]. The transport properties of metals are governed by their electronic structure in the energy range of several k_BT around the Fermi energy. In all investigated compounds the main contribution to the DOS near the Fermi energy originates from the d states of the rare earth, forming at those energies a series of peaks

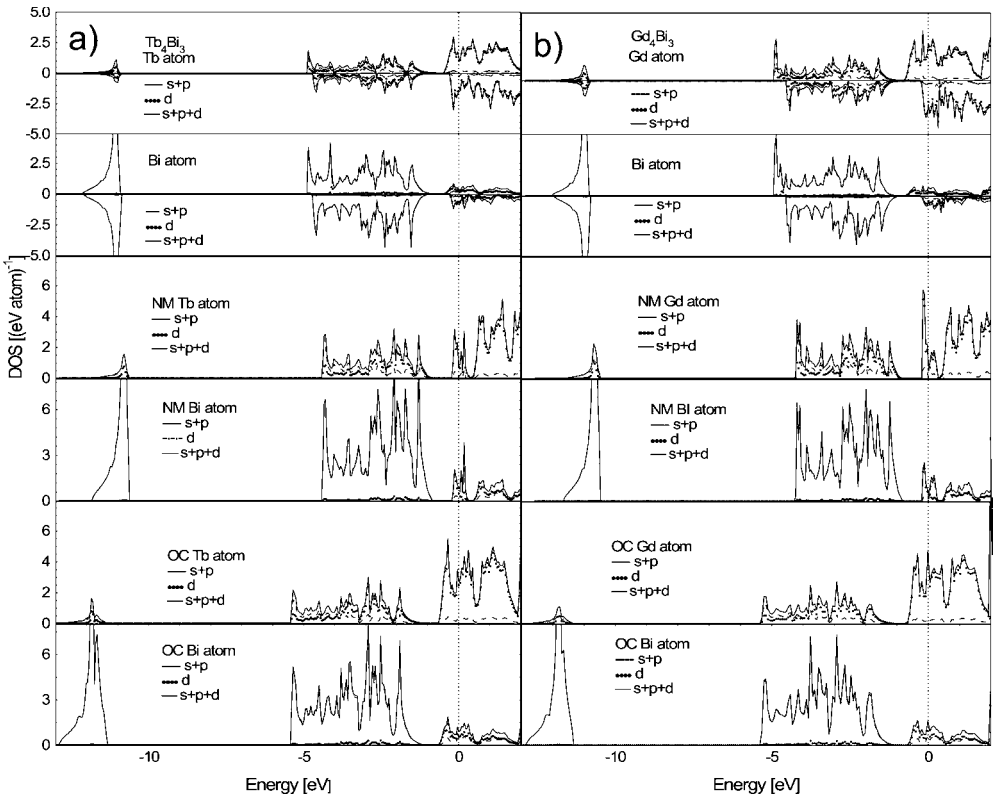

Figure 8. (a) Spin-resolved and orbital-decomposed atomic DOS contributed by Tb and metalloid Bi atoms obtained with the use of all methods for Tb_4Bi_3. Thin solid, dashed and thick solid curves depict respectively the s, s + p and s + p + d spin DOS. Vertical, dotted lines show the position of ε_F. (b) Spin-resolved and orbital-decomposed atomic DOS contributed by Gd and metalloid Bi atoms obtained with the use of all methods for Gd4Bi_3. Thin solid, dashed and thick solid curves depict respectively the s, s + p and s + p + d spin DOS. Vertical, dotted lines show the position of ε_F.

and dips, resulting in the highly non-uniform DOS. The energy gap lies too deep to influence the resistivity behaviour but the highly structured DOS of Gd (Tb) d states may influence the transport properties.

The results of calculation for R_5Bi_3 compounds are collected in figure 10 and in table 2. The shape of the DOS is in general similar to the compounds with the stoichiometry 4:3. There is a gap located at about 1 eV but its width is much smaller than for Gd_4Bi_3. The maximum of the DOS is located at about 2–2.5 eV below the Fermi level. The band crossing the Fermi level is built mainly from rare earth d states. This band gives also the main contribution to the polarization of the conduction states. It reaches about 0.3 μ_B for Gd_4Bi_3 and Gd_5Bi_3 (tables 1 and 2) although the exchange splitting is smaller in Gd_5Bi_3. The total DOS at the Fermi energy is however larger for the 4:3 compound (tables 1 and 2). It is worth mentioning that the low values of the DOS obtained for the non-magnetic case are the effect of the hybridization gap which is formed due to the 4f–d and 4f–sp hybridization which is unphysical for this kind of calculation. Analysis of the partial atomic contributions to the spin-polarized DOS of Gd_5Bi_3 (figure 11) shows that similarly to Gd_4Bi_3 the narrow band at about -12 eV comes from the 6s states of Bi. The valence band is composed of the strongly hybridized Gd d and Bi p states. The conduction band is dominated by the d states of Gd and shifted to higher BE as compared

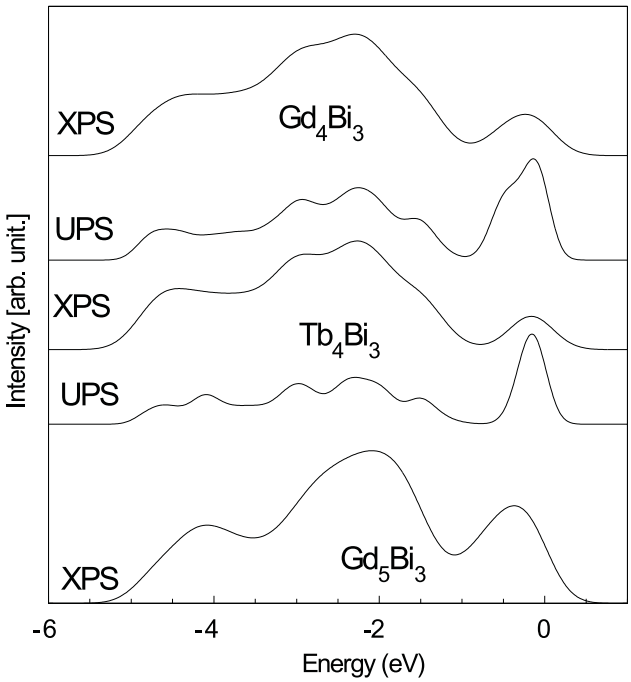

Figure 9. Simulated XPS and UPS spectra of Gd_4Bi_3, Tb_4Bi_3 and Gd_5Bi_3.

to Gd_4Bi_3. The overlap of the minority spin valence band with the majority spin conduction band reduces the width of the energy gap (figures 10 and 11).

The detailed analysis of the quantitative results obtained for the 5:3 compounds (table 2) indicates that the calculated parameters (state populations and partial magnetic moments) for various atomic positions of the same element are close each to another. The exception is the atomic charge polarization in Gd_5Bi_3 which varies from one position to another indicating to a significant dependence of the atomic charge on the crystal structure and atomic radius taken for the calculation. This seems to be a reason for the sign of the calculated charge transfer for most R_5Bi_3 compounds which cannot be compared to the experimental chemical shift from the XPS results. The exception is Dy_5Bi_3 for which the calculations have shown the sign of the charge transfer opposite to the rest of R_5Bi_3 compounds but in agreement with the experimental chemical shift. In this context it is worth mentioning that the experimental photoemission spectrum near the Fermi level differs for Dy_5Bi_3 from other compounds showing a pronounced bump at about 0.5 eV (figure 4). There is no indication in the calculations for such behaviour. The photoemission final states of the 4f shell, that are present in the spectra of Tb, Dy and Ho compounds, make the comparison to the calculations complicated in the spectral region above 3 eV BE.

For R_5Bi_3 only the spin-polarized mode of calculation has been performed. Figure 10 shows a clear dependence of the valence band exchange splitting on the spin of the 4f shell. One can also notice various behaviours of DOS in the vicinity of the Fermi level. For every compound there are dips or sharp structures of DOS for both spin directions. Such shape may be related to the temperature-dependent magnetic properties. Experiment has shown several unusual features such as a very large thermomagnetic effect for Dy_5Bi_3 or negative magnetization in a limited temperature range for Ho_5Bi_3 [5]. It is known that a large value of the derivative of the DOS in the vicinity of the Fermi edge may cause magnetic transitions.

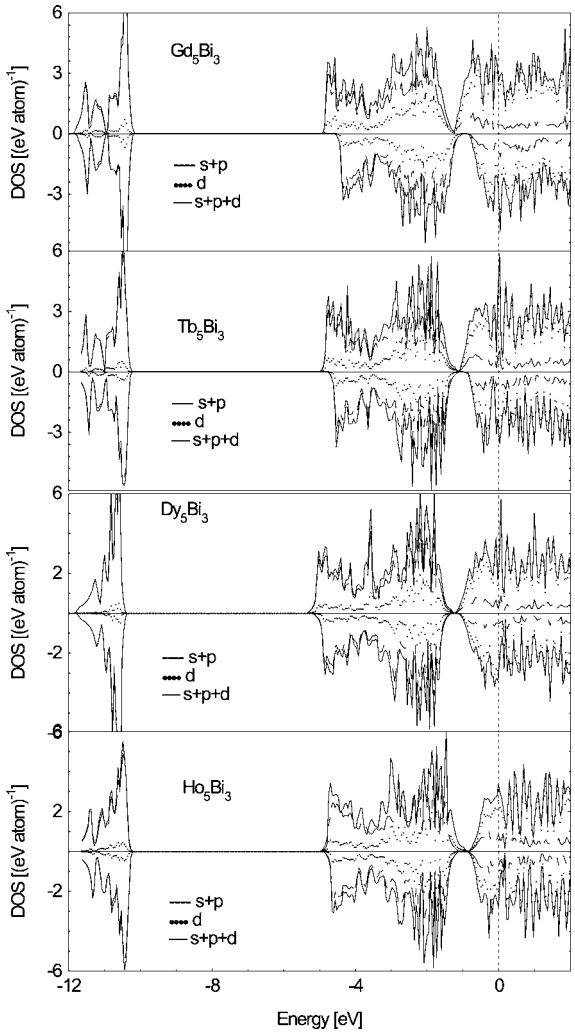

Figure 10. Total spd DOS of R_5Bi_3 (R = Gd, Tb, Dy and Ho) with separated orbital contributions. Vertical, dotted lines show the position of ε_F. The f states from R are not shown.

Figure 9 shows the XPS and UPS spectra simulated on the basis of the calculated partial densities of states (PDOS). The 4f state contributions have not been taken into account. The calculated spectra agree qualitatively with the experimental ones mainly in the XPS regime.

For the Gd_4Bi_3 compound the simulated XPS and UPS spectra consist of few features located at BEs of 4, 2.5, 2, 1.5 and 0.25 eV. The positions of the features and their relative intensities agree with the experimental XPS and UPS. The valley of low intensity, visible in both calculated (XPS, UPS) spectra, is due to the presence of the energy gap in the DOS of this compound (figures 7(b) and 8(b)). The main contribution to the simulated spectra comes from the d states of gadolinium and p states of Bi. The strong increase observed in the calculated UPS intensity at low BE, visible also for Tb_4Bi_3, comes from the very large photoionization cross section for rare earth 5d states at low photon energy (40.8 eV) [15]. The experimental UPS spectra show such an increase in relation to the XPS regime but it is less remarkable than in the model spectra. The cross sections taken for calculations have been obtained for atomic

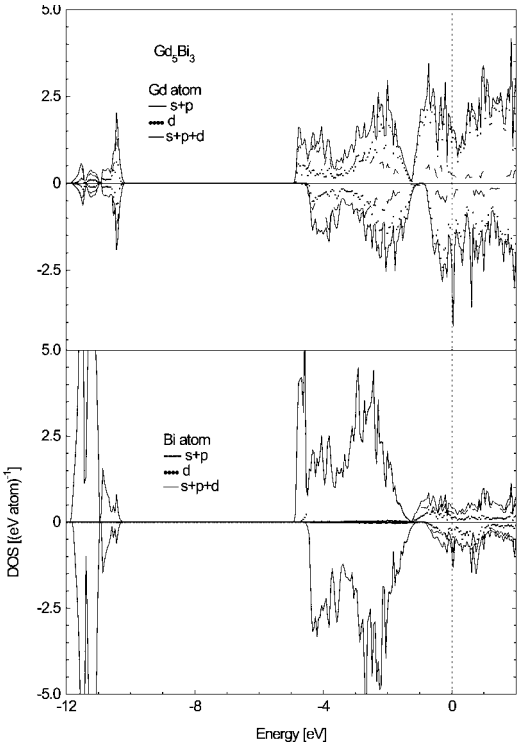

Figure 11. Spin-resolved and orbital-decomposed average atomic DOS contributed by four Gd and two metalloid Bi atoms for Gd_5Bi_3. Thin solid, dashed and thick solid curves depict respectively the s, s + p and s + p + d spin DOS. Vertical, dotted lines show the position of ε_F.

orbitals whereas the orbital character of the valence states is only partly retained, especially when hybridization takes place. The calculations concern the bulk states; however, one has to remember that the UPS spectra may contain a significant contribution from the surface states which cannot be analysed with the used method of band structure calculations. It may be a reason for some discrepancies between the experimental and modelled spectra.

4. Conclusions

A detailed analysis of the electronic structure of rare earth bismuthides has been performed based on photoelectron spectroscopy and band structure calculations. Both spectroscopic measurements and band calculations revealed the presence of an energy gap (at BE of 1 eV) separating the valence and conduction bands of investigated compounds. Calculations have shown that, while the valence band is built mainly of Bi 6p states, the conduction band is formed by d states of gadolinium. The presence of the energy gap in compounds with similar stoichiometry and different crystal structures suggests that mainly bismuth is responsible for the shape and location of the valence band, which is clearly separated from the Fermi energy.

The band structure of the investigated compounds can be understood by comparing with the shape and location of the bands of elemental components. The spectroscopic measurements showed that the photoemission spectra of Bi semi-metal is characterized by the valence band located well below the Fermi level [4]. On the other hand the bottom of the almost empty conduction spd bands of rare earth metals (for Gd see e.g. [16]) falls in the energy region of

the upper part of the Bi sp valence band. Due to the hybridization of the rare earth spd states with the Bi p states the valence band contracts and shifts to higher BE while the conduction band moves towards the Fermi level.

The formation of the energy gap observed in the investigated compounds may be the effect of 'band repulsion' driven by the hybridization interaction.

The interesting point is that the observed effects of energy band creation are driven mainly by the formation of the rare earth–bismuth compound independently of the crystal structure. Comparison between two groups of compounds with different crystal structures justifies the conclusion that the shape of the electronic bands is a result of R–Bi compound formation, whereas the details of the electronic structure as a DOS at the Fermi level drive the magnetic behaviour. The composition and the structure of the DOS in the vicinity of the Fermi level can result in untypical resistivity behaviour observed in the investigated compounds.

Based on the electronic structure calculations we could relate the temperature variation of the spectra in the vicinity of the magnetic transitions to the exchange splitting of the valence and conduction states.

References

[1] Yamada H, Fukawa T, Muro T, Tanaka Y, Imada S, Suga S, Li D X and Suzuki T 1996 *J. Phys. Soc. Japan* **65** 1000

[2] Li D X, Haga Y, Shida H, Suzuki T, Kwon Y S and Kido G 1997 *J. Phys.: Condens. Matter* **9** 10777

[3] Li D X, Haga Y, Shida H, Suzuki T and Kwon Y S 1996 *Phys. Rev.* B **54** 10483

[4] Szade J and Drzyzga M 2000 *J. Alloys Compounds* **299** 72

[5] Drzyzga M and Szade J 2001 *J. Alloys Compounds* **321** 27

[6] Szade J, Karla I, Gravel D and Neumann M 1999 *J. Alloys Compounds* **286** 153

[7] Szade J and Neumann M 1999 *J. Phys.: Condens. Matter* **11** 3887

[8] Andersen O K and Jepsen O 1984 *Phys. Rev. Lett.* **53** 2571
Andersen O K, Jepsen O and Glötzel D 1985 *Highlights of Condensed Matter Theory* ed F Bassani, F Fumi and M P Tosi (Amsterdam: North-Holland) p 59
Jepsen O and Andersen O K 1971 *Solid State Commun.* **9** 1763

[9] von Barth V and Hedin L 1972 *J. Phys. C: Solid State Phys.* **5** 1629

[10] Deniszczyk J and Borgieł W 1997 *J. Phys.: Condens. Matter* **9** 2187

[11] Langreth D C and Mehl M J 1981 *Phys. Rev.* B **28** 1809
Hu C D and Langreth D C 1985 *Phys. Scr.* **32** 391

[12] Blöchl P E, Jepsen O and Andersen O K 1994 *Phys. Rev.* B **49** 16223

[13] Yeh J and Lindau I 1985 *At. Data Nucl. Data Tables* **32** 1

[14] Ślebarski A, Maple M B, Freeman E J, Sirvent C, Tworuszka D, Orzechowska M, Wrona A, Jezierski A, Chiuzbaian S and Neumann M 2000 *Phys. Rev.* B **62** 3296

[15] Skorek G, Deniszczyk J, Szade J and Tyszka B 2001 *J. Phys.: Condens. Matter* **13** 6397

[16] Borgieł W, Borstel G and Nolting W 1986 *Solid State Commun.* **60** 313